Hamiltonian short-time critical dynamics of the three-dimensional XY model

Lindiane C. de Souza and Adauto J. F. de Souza
Departamento de Física, Universidade Federal Rural de Pernambuco, 52171-900, Recife PE, Brazil

Marcelo L. Lyra
Instituto de Física, Universidade Federal de Alagoas, 57072-970, Maceió AL, Brazil

(Received 19 December 2018; published 6 May 2019)

The short-time relaxation critical behavior of the XY model on a simple-cubic lattice is investigated within the scope of deterministic Hamiltonian dynamics. The Hamiltonian includes a first-neighbor interaction between planar vectors and a rotational kinetic term from which the motion equations are derived. The dynamical evolution from a fully ordered initial state is followed by employing a symplectic algorithm based on a high-order Trotter-Suzuki decomposition of the time-evolution operator. A finite-time scaling analysis is performed to provide accurate estimates of the critical energy density, the order-parameter relaxation exponent, and the dynamical critical exponent. The estimated critical exponents are consistent with prior theoretical and experimental values reported for the superfluid ^{4}He, extreme type-II superconducting, and Bose-Einstein condensation transitions.

DOI: 10.1103/PhysRevE.99.052104

I. INTRODUCTION

Studies of phase transitions taking place in systems with a two-component (XY) order parameter have played a long-standing role in condensed matter and statistical physics due to their unique properties and close relation with several key physical phenomena. In two dimensions, this system depicts an infinite-order Berezinskii-Kosterlitz-Thouless transition from a phase with bounded vortex-antivortex pairs to a phase with unpaired vortices [1,2]. In three dimensions, it exhibits a second-order spontaneous symmetry-breaking phase transition. Monte Carlo simulations combined with finite-size scaling methods and high-temperature expansions have provided accurate estimates for the full set of equilibrium critical exponents, including those associated with the singular behavior of the order parameter $\beta = 0.3485(2)$, susceptibility $\gamma = 1.3177(5)$, specific heat $\alpha = -0.0146(8)$, and correlation length $\nu = 0.671\,55(27)$ [3]. Physical realizations of this universality class phase transition are found in the superfluid λ transition in ^{4}He [4,5], in extreme type-II superconductors [6], and in the Bose-Einstein condensation of trapped atoms [7].

The critical dynamics of the three-dimensional (3D) XY model is influenced by the presence or not of conserved quantities [8]. In the case of pure relaxational dynamics, the dynamic critical exponent z governing the relaxation time needed to establish a diverging correlation length ($\tau \propto \xi^z$) is $z \simeq 2$. On the other hand, in the presence of a conserved density coupled to a spin-wave mode, the exact value $z = 3/2$ has been derived from renormalization-group arguments. This prediction has been corroborated by exploring the duality between the extreme type-II superconductor and a model with a critically fluctuating gauge field [9]. Recent experiments with ^{87}Rb atoms trapped in a cylindrical optical-box have probed the critical relaxation dynamics of the 3D Bose-Einstein condensation and supported the above prediction of $z = 3/2$ [10]. Measurements of the fluctuation conductivity in the superconductor $YBa_2Cu_3O_{7-\delta}$ are also consistent with this theoretical value [11,12].

The critical dynamics of the 3D XY universality class has also been probed by numerical simulations. Finite-size scaling studies of the linear resistance in a three-dimensional superconductor lattice model in the London limit have estimated $z = 1.51$ based on Monte Carlo simulations of the vortex loop dynamics [13]. Simulations of the Hamiltonian dynamics of the 3D XY model under thermal noise have given additional support for $z = 3/2$ when the dynamics conserves the local current [14,15]. For the case of relaxational dynamics, the dynamic exponent depends on the boundary conditions. $z = 2$ for periodic boundary conditions while $z = 3/2$ for fluctuating twisted boundary conditions due to the slower dynamics of the vortex loops imposed by such boundary condition, as discussed in detail in Refs. [14,15]. These simulations were performed on $L \times L \times L$ cubic lattice sizes up to $L = 32$ and addressed the finite-size scaling of the resistance and pair correlation function in the equilibrium state [14]. Further, the authors considered the system coupled to a thermal bath, which makes the dynamical process stochastic.

An alternative approach to study interacting many-body systems is to consider it isolated from the environment and evolving through its own deterministic Hamiltonian motion equations. In this case, the total energy is a constant of motion. However, other macroscopic quantities relax in time when their initial values are not the equilibrium ones. This approach has been successfully used to study the static critical properties of the ϕ^4 and XY models in two- and three-dimensional lattices [16–18]. Purely Hamiltonian dynamical processes toward equilibrium have also been explored to demonstrate that short-time critical relaxation studies can provide reliable estimates of static and dynamic critical exponents [19–22]. It

is worth stressing that the Hamiltonian approach is based on the fundamental deterministic motion equations for the microscopic degrees of freedom, in contrast with the stochastic artificial dynamics usually employed in Monte Carlo simulations. As such, it does not require any hypothesis of ergodicity and mixing usually assumed by construction in Monte Carlo dynamics. However, due to the high computational cost of directly integrating the microscopic motion equations, most studies of the critical Hamiltonian relaxation in three dimensions are restricted to small lattice sizes and/or very short times, which may contaminate the estimate of the critical parameters due to possible corrections to scaling.

In the present work, we provide an extensive study of the short-time purely Hamiltonian relaxation process of the XY model in $L \times L \times L$ cubic lattices. By employing an efficient parallel implementation of the Suzuki-Trotter decomposition of the time-evolution microscopic operators, we are able to follow the critical dynamics in lattices with $L = 256$, typically one order of magnitude larger than in previous studies of the 3D XY model. Starting from a configuration with fully aligned vectors with randomly distributed angular momenta, we use a finite-time scaling analysis of the order parameter to precisely determine the critical energy density. The time evolution of relevant macroscopic quantities at the critical energy gives accurate estimates of dynamic critical exponents. These are compared with the best Monte Carlo estimates available in the literature.

II. THE 3D XY MODEL HAMILTONIAN AND MOTION EQUATIONS

We will consider a system of interacting planar rotators with an intrinsic rotational inertia. The orientational degree of freedom of the ith rotator is characterized by the angle $\theta_i \in [-\pi, +\pi]$, with p_i representing its angular momentum. The rotators will be assumed to be located at the sites of a cubic lattice of lateral size L. The model Hamiltonian including the interaction potential and kinetic energy can be written as

$$\mathcal{H} = -J \sum_{\langle i,j \rangle} \cos(\theta_i - \theta_j) + \sum_i \frac{p_i^2}{2I}, \tag{1}$$

where $\langle i, j \rangle$ represent all pairs of neighboring sites. J is the typical strength of the coupling between nearest-neighbor rotators, and I is the moment of inertia. In what follows, we will use time and momentum scales of $J = I = 1$ without any loss of generality.

The motion equations for the set of generalized coordinates $y(t) = \{\theta_i(t), p_i(t)\}$ follow from the usual Hamilton equations,

$$\dot{\theta}_i = \frac{\partial \mathcal{H}}{\partial p_i}, \tag{2}$$

$$-\dot{p}_i = \frac{\partial \mathcal{H}}{\partial \theta_i}. \tag{3}$$

The above motion equations can be put in a simple form in terms of a Liouville operator as $\dot{y}(t) = \hat{L} y(t)$ with

$$\hat{L} = \sum_{i=1}^{N} \left(\frac{\partial \mathcal{H}}{\partial p_i} \frac{\partial}{\partial \theta_i} - \frac{\partial \mathcal{H}}{\partial \theta_i} \frac{\partial}{\partial p_i} \right) \equiv \hat{A} + \hat{B}, \tag{4}$$

where we introduced the noncommuting operators

$$\hat{A} = \sum_{i=1}^{N} \frac{\partial \mathcal{H}}{\partial p_i} \frac{\partial}{\partial \theta_i} \tag{5}$$

and

$$\hat{B} = -\sum_{i=1}^{N} \frac{\partial \mathcal{H}}{\partial \theta_i} \frac{\partial}{\partial p_i}. \tag{6}$$

The Liouville equation can be formally solved as

$$y(t + \Delta) = e^{(\hat{A}+\hat{B})\Delta} y(t), \tag{7}$$

where Δ is a given time step. Due to the noncommuting nature of the operators $\hat{A}$ and $\hat{B}$, the action of the total evolution operator becomes nontrivial. However, the separate action of each term can be easily expressed as

$$e^{\hat{A}\Delta}\{\theta_i, p_i\} = \{\theta_i + p_i \Delta, p_i\} \tag{8}$$

and

$$e^{\hat{B}\Delta}\{\theta_i, p_i\} = \{\theta_i, p_i + \alpha_i \Delta\} \tag{9}$$

where $\alpha_i = \sum_{j(i)} \sin(\theta_i - \theta_j)$ with the sum running over all sites j that are first neighbors of site i.

One strategy to integrate the motion equations is to perform a Suzuki-Trotter decomposition of the exponential evolution operator [23]. The simplest decomposition is

$$e^{(\hat{A}+\hat{B})\Delta} = e^{\hat{A}\Delta} e^{\hat{B}\Delta} + O(\Delta^2), \tag{10}$$

with an error of the order of Δ^2 for noncommuting operators. The above decomposition of the exponential operator has a remarkable advantage when compared with the other approximants based on a power-series expansion of the left-hand side of Eq. (10). Such a decomposition is time-reversible, keeping the error in total energy bounded, and it conserves the volume in phase space. Therefore, the resulting numerical integrator is symplectic by construction. Conservation of energy and phase-space volume are valuable properties of numerical integrators and are intimately related to the stability and precision in long-time runs.

Improved decompositions of the exponential operator can be achieved by fractioning the evolution time [24,25]. In particular, a second-order decomposition can be written as

$$S_2(\Delta) = e^{\frac{\Delta}{2}\hat{A}} e^{\Delta\hat{B}} e^{\frac{\Delta}{2}\hat{A}} = e^{(\hat{A}+\hat{B})\Delta + O(\Delta^3)}. \tag{11}$$

Therefore, the time evolution of the system configuration can be simulated by $y(t + \Delta) = S_2(\Delta) y(t)$ with an error of the order of $O(\Delta^3)$. Notice that such decomposition still allows for the subsequent update of momentum and angle variables [see Eqs. (8) and (9)]. In what follows, we will use an even more precise fourth-order decomposition of the evolution exponential operator

$$S_4(x) = [S_2(s_2 x)]^2 S_2[(1 - 4s_2)x][S_2(s_2 x)]^2 \tag{12}$$

with $s_2 = 1/(4 - 4^{1/3})$ for which the decomposition error is $O(\Delta^5)$ [24,25]. With the above high-order decomposition, the momentum and angle variables can be updated in subsequent steps of the simulation $y(t + \Delta) = S_4(\Delta) y(t)$ without needing to use very small time steps as usually required when low-order decompositions are implemented.

The numerical procedure implied by Eq. (12) allows for a fully parallel implementation on the graphical card unit by using CUDA [26]. Besides, the time step Δ can be made much greater than those employed in other classes of integration algorithms. Applying (12) to a system state consists in executing Eqs. (8) and (9) alternately. In turn, the whole set of coordinates or momenta can be updated in parallel.

III. SHORT-TIME CRITICAL DYNAMICS: FINITE-TIME SCALING

Most studies of critical phenomena focus on the singular behavior of equilibrium thermodynamic quantities. However, the divergences of the typical correlation length and time scales at the critical point bring to computational studies the issue of the critical slowing down. The characteristic correlation time grows as $\tau \propto L^z$. Therefore, very long runs are needed to obtain a good ensemble of uncorrelated configurations necessary to perform the thermodynamic averages. Ultimately, the critical slowing down strongly restricts the simulated system sizes, and finite-size scaling arguments are usually developed to extract the relevant critical parameters.

Renormalization-group arguments have predicted that the dynamical evolution of a system prepared in a state far from equilibrium is also critical at a second-order transition [27]. This prediction has been confirmed in several studies of critical relaxation in a variety of physical systems [28–40]. According to this formulation, the order parameter at the critical point decays as $\langle M(t)\rangle \propto t^{-\beta/\nu z}$ when the system is initially prepared in a fully ordered state. Here $\langle\cdots\rangle$ represents an average over several realizations of the relaxation process. This power-law behavior develops after an initial transient microscopic time. In the vicinity of the critical point, the order parameter acquires the following scaling form:

$$\langle M(t,e)\rangle = t^{-\beta/\nu z}\mathcal{M}(t^{1/\nu z}\varepsilon), \tag{13}$$

where e is a control parameter and $\varepsilon = (e/e_c - 1)$ is the normalized distance to the critical point e_c. Notice that, in simulations in which the system is in contact with a thermal bath at temperature T, the distance to the critical point is measured as $(T/T_c - 1)$. In microcanonical simulations, the control parameter is the distance in energy to the critical point. These two measures can be related to each other in the equilibrium steady state in which the temperature can be related to the average kinetic energy. To locate the critical point, it is quite useful to introduce the auxiliary function

$$\Psi(t,e) = \frac{\partial \ln \langle M(t,e)\rangle}{\partial \ln t}. \tag{14}$$

The finite-time scaling hypothesis for the order-parameter relaxation implies that

$$\Psi(t,e) = -\frac{\beta}{\nu z} + g(t^{1/\nu z}\varepsilon), \tag{15}$$

with $g(t^{1/\nu z}\varepsilon) = \frac{\partial \ln \mathcal{M}(t^{1/\nu z}\varepsilon)}{\partial \ln t}$. Therefore, this auxiliary function becomes time-independent at the critical point $\varepsilon = 0$. Further, as $g(0) = 0$, the auxiliary function at the critical point $\Psi(t,0) = -\beta/\nu z$ for any time t in the scaling regime. In practice, all curves $\Psi(t_i,e)$ taken at distinct times t_i cross at a single point when plotted against e, simultaneously identifying the critical point e_c and the critical exponents ratio $\beta/\nu z$. Additionally, when these functions are plotted using the proper scaling variable $x = t^{1/\nu z}\varepsilon$, all curves collapse into a single curve. The data collapse procedure provides the critical exponents ratio $1/\nu z$.

It is worth mentioning that short-time critical dynamics also emerge from simulations starting from random configurations. In the case of an infinitesimal initial value of the order parameter, it develops a critical initial slip [27]. Recently, it has been demonstrated that such an initial slip can present the same dynamic exponent even for models having distinct stationary critical exponents [40]. In the next section, we will follow the Hamiltonian relaxation from the fully ordered initial configuration.

IV. THE HAMILTONIAN CRITICAL RELAXATION OF THE 3D *XY* MODEL: NUMERICAL RESULTS

In this section, we will report our numerical results for the Hamiltonian relaxation process of the order parameter near the critical point of the 3D XY model. In what follows, we considered a cubic lattice with periodic boundary conditions and lateral side $L = 256$, which is implied in a simulation with $N = 2^{24} \approx 1.7 \times 10^7$ coupled rotators. As the time evolution of the system is a Hamiltonian, the total energy is a constant of motion. The minimum energy per rotator is $e_{\min} = -3$, which corresponds to a state with rotators fully aligned and at rest. When energy is added to the system, it is distributed in the orientational and kinetic degrees of freedom. Above a critical energy e_c there is no orientational long-range order in the equilibrium state. Therefore, the energy density e acts as the control parameter in this class of Hamiltonian microcanonical simulations.

In our simulations, we fixed the energy density $e > e_{\min}$ and prepared the system in a fully ordered orientational state with $\theta_i = 0$. The remaining energy was distributed in the kinetic degrees of freedom by randomly choosing the angular momentum of each rotator from a Gaussian distribution with zero average. After that, we followed the time evolution of the system by directly integrating the motion equations using the fourth-order decomposition of the exponential evolution operator described in Sec. II. In our simulations, we used a time step $\Delta = 0.2$ for which the simulation errors were negligible for runs up to a total time $t_{\max} = 10^4$. The use of smaller time steps would enhance the computational time with no effective improvement of the simulation results within the statistical error bar. Integration errors started to become relevant for larger time steps. Averages were performed over 2048 distinct initial distributions of the rotators' angular momenta.

We considered the average magnitude of the magnetization $\langle M\rangle = \sqrt{\langle M_x\rangle^2 + \langle M_y\rangle^2}$ as a proper orientational order parameter, where $\langle M_\alpha\rangle$ is the average projection of the rotators along direction α [$\langle M_x\rangle = (1/N)\sum_{i=1}^N \cos\theta_i$; $\langle M_y\rangle = (1/N)\sum_{i=1}^N \sin\theta_i$]. In Fig. 1 we report our simulation results for the time evolution of the order parameter averaged over distinct initial conditions. Although we performed simulations over a wider range of energy densities, we are reporting just a few curves in the vicinity of the critical point. For energy densities below the critical point, the order parameter relaxes from the initial nonequilibrium state converging to a finite

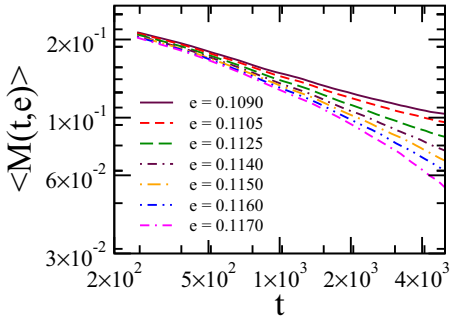

FIG. 1. Average order-parameter relaxation process. Data are for distinct energy densities in the vicinity of the critical point $e_c = 0.113\,38$ (see text). Below the critical energy, it starts to saturate signaling the setting up of a finite orientational order in the final equilibrium state. It develops a faster than power-law decay above the critical energy.

value signaling a sustainable orientational long-range order. Above the critical energy density, the amount of kinetic rotational energy is enough to fully destroy the orientational order, which vanishes exponentially fast. At the critical energy, the order parameter develops a slower power-law decay after a microscopic transient time. The very short-time relaxation is not shown to emphasize the scaling regime.

A clearer signature of the critical point is evidenced by plotting the time evolution of the auxiliary function $\Psi(t, e)$, as shown in Fig. 2. Below the critical energy, the auxiliary function approaches zero in the long-time regime due to the remaining long-range orientational order. On the other hand, it assumes diverging negative values above the critical point reflecting the exponential relaxation toward the nonordered equilibrium state. Just at the critical energy, it reaches a finite value. The reported data in Fig. 2 allow us to estimate that $0.1125 < e_c < 0.1140$.

To check that no significant finite-size effects are present in our simulation data, we computed the normalized pair correlation function $g(r) = (\langle \mathbf{M_i} \cdot \mathbf{M_{i+r}} \rangle - \langle M \rangle^2)/(\langle \mathbf{M_i} \cdot \mathbf{M_i} \rangle - \langle M \rangle^2)$ at distinct times for $e = 0.1125$. Our results are

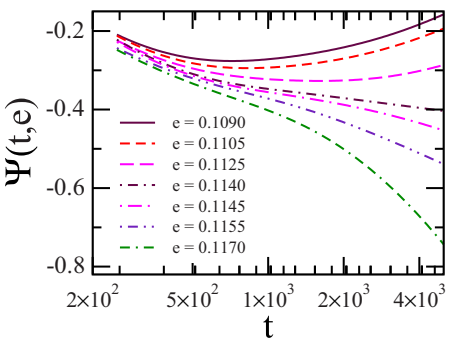

FIG. 2. Time evolution of the auxiliary function $\Psi(t, e)$ for distinct energy densities in the vicinity of the critical point $e_c = 0.113\,38$ (see the text). Below the critical energy density it converges to $\Psi(t \to \infty, e) \to 0$ when approaching the final equilibrium state. The reverse trend develops above the critical point with $\Psi(t \to \infty, e) \to -\infty$. At the critical energy, it is expected to saturate at a finite value according to the finite-time scaling hypothesis

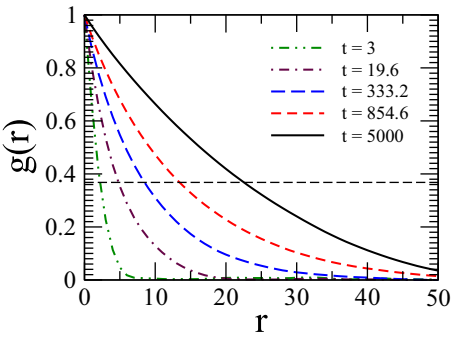

FIG. 3. Pair correlation function $g(r)$ as a function of r computed at $e = 0.1125$ (in the vicinity of the critical energy) and distinct evolution times. The horizontal thin dashed line corresponds to $g(\xi) = 1/e$. Notice that, in the longest run, ξ is still one order of magnitude smaller that the lattice size $L = 256$.

reported in Fig. 3 with r measured along a fixed direction. Notice that the correlation function presents a fast decay at very short times because the fluctuations are uncorrelated at the very beginning of the dynamic evolution starting from a fully ordered state. These are developed as time evolves. Assuming an exponential decay of the correlation function in the form $g(r) = \exp(-r/\xi)$, a rough estimate of the typical correlation length ξ can be found as $g(\xi) = \exp(-1)$, which is of the same order as that of the second-moment correlation length [41]. Therefore, although the correlation length grows in time, it remains at least one order of magnitude smaller than the linear size of the lattice used in our simulations.

To precisely locate the critical energy density, we followed the finite-time scaling hypothesis described in Sec. III and plotted $\Psi(t, e)$ as a function of e taken at distinct run times. Our results from energy densities around the critical point and a selected set of run times are reported in Fig. 4. A nice crossing point of all curves with a very narrow spread is a clear signature that no relevant corrections to scaling are present in the data. From this crossing, we could accurately estimate $e_c = 0.113\,38(8)$ and $\beta/\nu z = 0.350(5)$.

To estimate the critical exponents ratio $1/\nu z$, we performed a collapse of our data for $\Psi(t, e)$ by plotting them as a function of the proper scaling variable $x = t^{1/\nu z}(e/e_c - 1)$. Our result is summarized in Fig. 5. The critical exponent was chosen

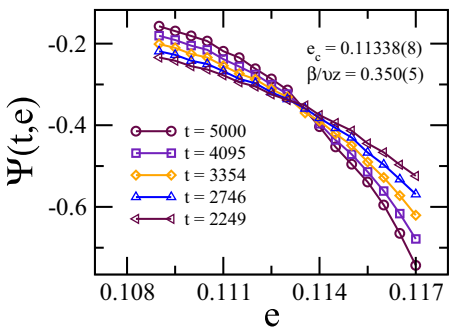

FIG. 4. The auxiliary function $\Psi(t, e)$ vs e taken at distinct times. All curves cross at a single point identifying the critical energy e_c and the exponent ratio $\beta/\nu z$. From this, we estimate $e_c = 0.113\,38(8)$ and $\beta/\nu z = 0.350(5)$.

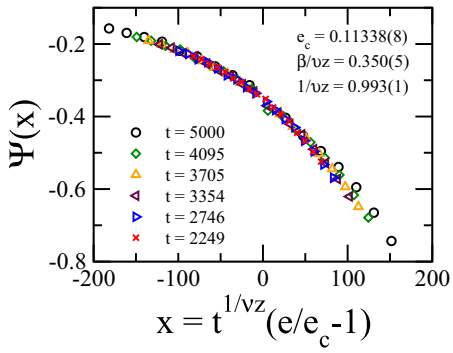

FIG. 5. The auxiliary function plotted against the proper scaling variable $x = t^{1/\nu z}(e/e_c - 1)$. The collapse of all curves supports the finite-time scaling hypothesis. The best collapse of data from distinct run times allowed us to estimate $1/\nu z = 0.993(1)$.

as that leading to the minimum spreading of the curves, especially in the vicinity of the critical point. Our best estimate gives $1/\nu z = 0.993(1)$.

The precision of the above estimates for the critical parameters can be further verified by collapsing data for their own magnetization. The scaling hypothesis implies that when plotting $t^{\beta/\nu z}\langle M(t,e)\rangle$ versus the scaling variable $t^{1/\nu z}(e/e_c - 1)$, all curves shall also collapse into a single curve. This scaling analysis is reported in Fig. 6 using the same critical parameters determined above. The fine collapse of all curves is an additional indication of the reliability of these estimates

To obtain a direct estimate of the dynamical critical exponent z, we followed the time evolution of the second-order cumulant defined as

$$U(t) = \frac{\left(\langle M_x^2\rangle + \langle M_y^2\rangle\right) - \left(\langle M_x\rangle^2 + \langle M_y\rangle^2\right)}{\langle M_x\rangle^2 + \langle M_y\rangle^2}. \qquad (16)$$

According to the finite-time scaling behavior, the second cumulant shall grow in time as $U_c(t) \propto t^{d/z}$ at the critical point, where d is the space dimension [37]. In Fig. 7 we report our simulation data for $U(t)$ at the critical energy density, which is consistent with $U_c(t) \propto t^2$. This behavior is in agreement with the renormalization-group prediction of $z = 3/2$ for the 3D

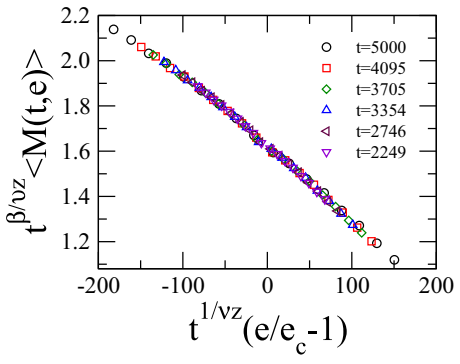

FIG. 6. Data collapse of the order-parameter data computed at distinct times and energy densities. The critical parameters are the same as those described in Fig. 5. The fine collapse of the curves corroborates the reliability of the estimated critical parameters.

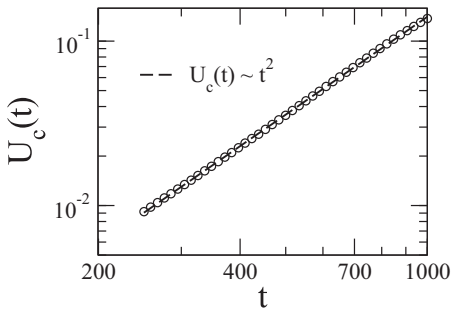

FIG. 7. Time evolution of the second cumulant $U(t)$ computed at the critical energy density. The dashed line corresponds to the power-law growth $U(t) \propto t^2$, which is consistent with exact calculations for the dynamical critical exponent $z = 3/2$.

XY model with a conserved density coupled to a spin-wave mode [8].

V. SUMMARY AND DISCUSSION

In summary, we performed large-scale simulations of the purely Hamiltonian critical relaxation of the XY model defined on a cubic lattice. The Hamiltonian was considered to include the kinetic energy of the rotators besides their first-neighbor ferromagnetic coupling. The Hamilton motion equations were numerically solved by using a high-order time-reversal decomposition of the exponential evolution operator, thus conserving the volume in phase space by construction. Within such a microcanonical approach, we accurately followed the short-time critical relaxation process from the fully orientationally ordered state.

We were able to simulate lattices as large as $L = 256^3$ sites for which finite-size effects were negligible during the finite integration time considered. The runs were long enough to probe the finite-time critical relaxation regime without the presence of significant corrections to scaling. By exploring the finite-time scaling hypothesis for the order parameter, we determined the critical energy density as $e_c = 0.113\,38(8)$ and the critical exponents ratios $\beta/\nu z = 0.350(5)$, $1/\nu z = 0.993(1)$. The critical energy density includes both orientational and kinetic contributions. Monte Carlo simulations performed in the canonical ensemble, with the system in equilibrium with a thermal bath, have estimated the transition to take place at $1/T_c = 0.454\,20(2)$ and a critical interaction energy per spin $E_c = -0.9890(3)$ [42,43]. Assuming that the average kinetic energy per rotator in equilibrium is $T/2$ according to the classical equipartition theorem, these values provide an estimate for the critical total energy density of $e_c = 0.1118(4)$, compatible with our present estimate. Further, the second-order cumulant time evolution showed that the critical dynamical exponent is consistent with the exact prediction of $z = 3/2$. From this set of exponents, our results provide the following estimates of the independent static critical exponents $\beta = 0.352(5)$ and $\nu = 0.671(1)$. These are very close to the best estimates based on Monte Carlo simulations $\beta = 0.3485(2)$ and $\nu = 0.671\,55(27)$ [3]. We would like to stress that the critical energy density of the 3D XY model is above the energy density of a configuration with rotators at rest with random and uncorrelated orientations. As such, the critical

initial slip of the order parameter from partially ordered initial states can be probed by such Hamiltonian microcanonical simulations. The critical dynamics of vortex loops and domain walls can also be addressed from similar fully deterministic simulations.

It is important to emphasize that the present results were derived from the intrinsic deterministic Hamiltonian dynamics of the system. In contrast, Monte Carlo simulations use artificial stochastic dynamics that drive the system toward the thermodynamic equilibrium state by imposing the detailed balance condition. Within this scenario, the present results add to the recent developments of advanced computational strategies, reaching the stage to accurately probe critical phenomena directly from first-principles simulations based on symplectic integration protocols that preserve the relevant symmetries of the underlying microscopic dynamics.

ACKNOWLEDGMENTS

This work was supported by CAPES (Coordenação de Aperfeiçoamento de Pessoal de Nível Superior), CNPq (Conselho Nacional de Desenvolvimento Científico e Tecnológico), FAPEAL (Fundação de Apoio à Pesquisa do Estado de Alagoas), and FACEPE (Fundação de Amparo à Ciência e Tecnologia do Estado de Pernambuco). M.L.L. acknowledges the hospitality of the Physics Department of Federal University of Pernambuco where this work has been developed with partial financial support from a partnership program CAPES/FACEPE (Grant No. APQ-0325-1.05/18).

[1] V. L. Berezinskii, Zh. Eksp. Teor. Fiz. **59**, 907 (1970) [Sov. Phys. JETP **32**, 493 (1971)].
[2] J. M. Kosterlitz and D. J. Thouless, J. Phys. C **6**, 1181 (1973).
[3] M. Campostrini, M. Hasenbusch, A. Pelissetto, P. Rossi, and E. Vicari, Phys. Rev. B **63**, 214503 (2001).
[4] J. A. Lipa and T. C. P. Chui, Phys. Rev. Lett. **51**, 2291 (1983).
[5] J. A. Lipa, D. R. Swanson, J. A. Nissen, T. C. P. Chui, and U. E. Israelsson, Phys. Rev. Lett. **76**, 944 (1996).
[6] M. B. Salamon, J. Shi, N. Overend, and M. A. Howson, Phys. Rev. B **47**, 5520 (1993).
[7] T. Donner, S. Ritter, T. Bourdel, A. Öttl, M. Köhl, and T. Esslinger, Science **315**, 1556 (2007).
[8] P. C. Hohenberg and B. I. Halperin, Rev. Mod. Phys. **49**, 435 (1977).
[9] F. S. Nogueira and D. Manske, Phys. Rev. B **72**, 014541 (2005).
[10] N. Navon, A. L. Gaunt, R. P. Smith, and Z. Hadzibabic, Science **347**, 167 (2015).
[11] K. Moloni, M. Friesen, S. Li, V. Souw, P. Metcalf, L. Hou, and M. McElfresh, Phys. Rev. Lett. **78**, 3173 (1997).
[12] J.-T. Kim, N. Goldenfeld, J. Giapintzakis, and D. M. Ginsberg, Phys. Rev. B **56**, 118 (1997).
[13] H. Weber and H. J. Jensen, Phys. Rev. Lett. **78**, 2620 (1997).
[14] L. M. Jensen, B. J. Kim, and P. Minnhagen, Europhys. Lett. **49**, 644 (2000).
[15] L. M. Jensen, B. J. Kim, and P. Minnhagen, Phys. Rev. B **61**, 15412 (2000).
[16] X. Leoncini, A. D. Verga, and S. Ruffo, Phys. Rev. E **57**, 6377 (1998).
[17] M. Cerruti-Sola, C. Clementi, and M. Pettini, Phys. Rev. E **61**, 5171 (2000).
[18] L. Caiani, L. Casetti, and M. Pettini, J. Phys. A **31**, 3357 (1998).
[19] B. Zheng, M. Schulz, and S. Trimper, Phys. Rev. Lett. **82**, 1891 (1999).
[20] B. Zheng, Phys. Rev. E **61**, 153 (2000).
[21] R. H. Dong, B. Zheng, and N. J. Zhou, Europhys. Lett. **99**, 56001 (2012).
[22] A. Asad and B. Zheng, J. Phys. A **40**, 9957 (2007).
[23] N. Hatano and M. Suzuki, *Finding Exponential Product Formulas of Higher Orders* (Springer, Berlin, 2005).
[24] M. Suzuki, Phys. Lett. A **146**, 319 (1990).
[25] M. Suzuki, Physica A **205**, 65 (1994).
[26] S. Cook, *CUDA Programming: A Developer's Guide to Parallel Computing with GPUs* (Morgan Kaufmann, San Francisco, 2013).
[27] H. K. Janssen, B. Schaub, and B. Schmittmann, Z. Phys. B **73**, 539 (1989).
[28] B. Zheng, Int. J. Mod. Phys. B **12**, 1419 (1998).
[29] L. Schulke and B. Zheng, Phys. Lett. A **204**, 295 (1995).
[30] T. Tome and M. J. de Oliveira, Phys. Rev. E **58**, 4242 (1998).
[31] R. da Silva, N. A. Alves, and J. R. Drugowich de Felicio, Phys. Rev. E **66**, 026130 (2002).
[32] L. Schulke and B. Zheng, Phys. Lett. A **215**, 81 (1996).
[33] U. Ritschel and P. Czerner, Phys. Rev. Lett. **75**, 3882 (1995).
[34] X. W. Lei and B. Zheng, Phys. Rev. E **75**, 040104(R) (2007).
[35] C. M. Horowitz, M. A. Bab, M. Mazzini, M. L. Rubio Puzzo, and G. P. Saracco, Phys. Rev. E **92**, 042127 (2015).
[36] Y.-R. Shu, S. Yin, and D.-X. Yao, Phys. Rev. B **96**, 094304 (2017).
[37] E. V. Albano, M. A. Bab, G. Baglietto, R. A. Borzi, T. S. Grigera, E. S. Loscar, D. E. Rodriguez, M. L. Rubio Puzzo, and G. P. Saracco, Rep. Prog. Phys. **74**, 026501 (2011).
[38] Y. Hotta, Phys. Rev. E **93**, 062136 (2016).
[39] U. Basu, V. Volpati, S. Caracciolo, and A. Gambassi, Phys. Rev. Lett. **118**, 050602 (2017).
[40] V. Volpati, U. Basu, S. Caracciolo, and A. Gambassi, Phys. Rev. E **96**, 052136 (2017).
[41] M. Hasenbusch, Phys. Rev. B **82**, 174434 (2010).
[42] A. P. Gottlob and M. Hasenbusch, Physica A **201**, 593 (1993).
[43] R. Nerattini, A. Trombettoni, and L. Casetti, J. Stat. Mech. (2014) P12001.